

Simulation and design of shaped pulses beyond the piecewise-constant approximation

Uluk Rasulov, Anupama Acharya,
Marina Carravetta, Ilya Kuprov*

School of Chemistry, University of Southampton, United Kingdom

*i.kuprov@soton.ac.uk

Abstract

Response functions of resonant circuits create ringing artefacts if their input changes rapidly. When physical limits of electromagnetic spectroscopies are explored, this creates two types of problems. Firstly, simulation: the system must be propagated accurately through every response transient, this may be computationally expensive. Secondly, optimal control optimisation: instrument response must be taken into account; it may be advantageous to design pulses that are resilient to instrumental distortions. At the root of both problems is the popular piecewise-constant approximation for control sequences; in magnetic resonance it has persisted since the earliest days. In this paper, we report an implementation and benchmarks for simulation and optimal control routines that use recent Lie-group methods that simulate and optimise control pulses that are piecewise-polynomial.

1. Introduction

The original formulation [1] and many subsequent refinements [2-4] of the gradient ascent pulse engineering (GRAPE) method for quantum optimal control use the piecewise-constant approximation for the control Hamiltonian. GRAPE also makes an unstated assumption that hardware response functions (amplifiers, lasers, cavities, *etc.*) create negligible distortions in the control sequence. When this approximation holds, for example in liquid state nuclear magnetic resonance (NMR) [5,6] and atom interferometry [7,8], optimal control theory yields impressive results. Some instrumental effects, such as wire distance modulation in magic angle spinning NMR, can be accurately accounted for [9] within the piecewise-constant approximation. However, there are cases where – in our hands and in the unpublished experience of other groups – theoretically optimal piecewise-constant GRAPE control sequences inexplicably fail to generate the desired dynamics in experimental systems.

One likely reason is illustrated in Figure 1 for a typical composite radiofrequency pulse used in ^{14}N NMR spectroscopy. The significant distortion introduced by the probe circuit prevents the control sequence from taking the ensemble of ^{14}N spins to the intended destination state.

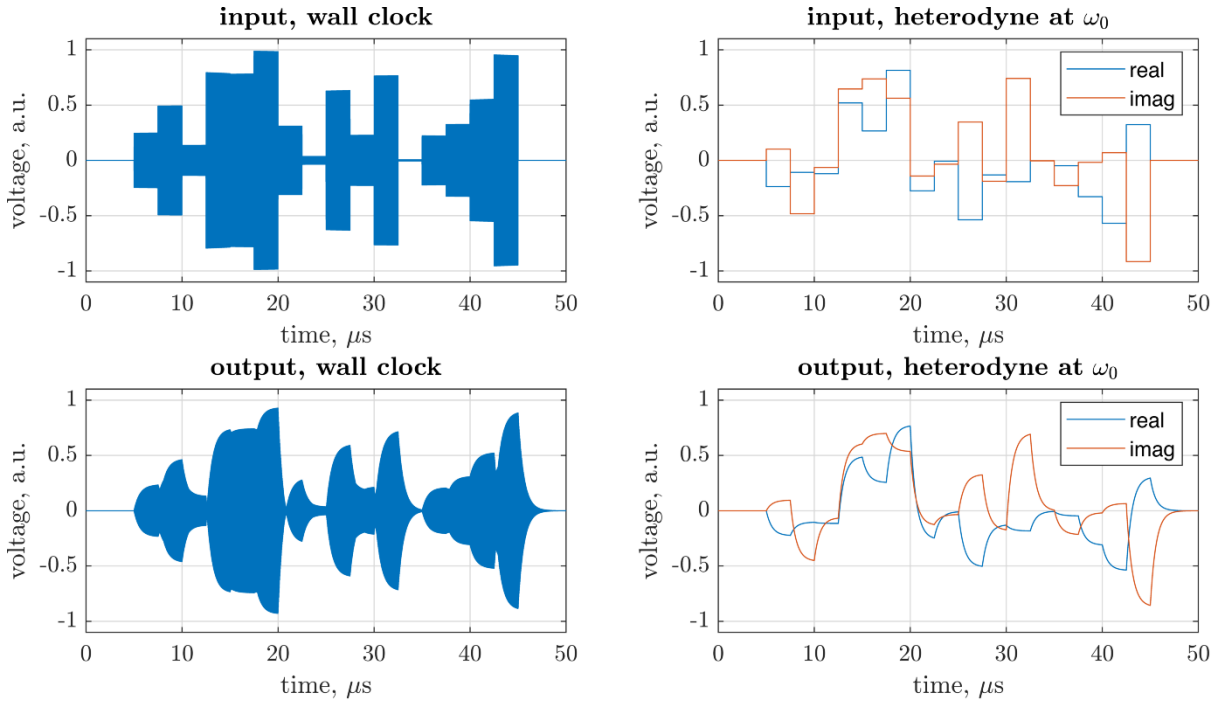


Figure 1. Distortions created in a composite pulse by a nuclear magnetic resonance probe tuned to the ^{14}N spin precession frequency in a 14.09 Tesla magnet. The probe is modelled, using Spinach 2.7 [10], as a lumped RLC circuit with a quality factor $Q = 80$. **Top Left:** input voltage as a function of time; oscillations at 43.36 MHz appear as solid blocks. **Top Right:** rotating frame representation of the same pulse, indicating the in-phase (blue line) and out-of-phase (red line) components relative to the $\omega_0/2\pi = 43.37$ MHz reference frequency. **Bottom Row:** same quantities plotted after convolution with the response function of the probe RLC circuit.

Such distortions can sometimes be ignored: they diminish for higher frequencies and smaller quality factors, they may also be tolerated because the definition of a GRAPE optimum [1] is zero derivative (meaning first-order resilience) of the fidelity with respect to small variations in the control sequence. Still, there are cases – notably, quadrupolar NMR and time-domain EPR spectroscopy – where anecdotal evidence indicates that instrument response functions destroy the efficiency advantages

predicted by idealised GRAPE optimisations. Figure 1 suggests that the reason is the presence of response transients at the edges of the pulse sequence. An obvious solution would be to create a sequence without such edges: to move from a piecewise-constant to at least piecewise-linear, and possibly to appropriately stitched piecewise-polynomial model.

2. Two- and three-point product integrators

The idea of moving the shaped pulse model from piecewise-constant to piecewise-linear strikes down the first approximation made in foundational texts on numerical magnetic resonance simulation [11,12] and optimal control [1,13] – time slicing followed by the assumption that the Hamiltonian does not change within a sufficiently thin slice. Mathematically speaking, we would be moving away from the picture where the time-ordered exponential [14] expression for the propagator $\mathcal{P}(t)$:

$$\begin{aligned} \frac{d}{dt} \mathbf{p}(t) &= -i\mathcal{L}(t)\mathbf{p}(t), & \mathcal{L}(t) &= \mathcal{H}(t) + i\mathcal{R} + \dots \\ \mathbf{p}(t) &= \mathcal{P}(t)\mathbf{p}(0), & \mathcal{P}(t) &= \overleftarrow{\exp} \left(-i \int_0^t \mathcal{L}(t) dt \right) \end{aligned} \quad (1)$$

is approximated by a product integral – as the zero slice width limit of a time-ordered product:

$$\overleftarrow{\exp} \left(-i \int_0^t \mathcal{L}(t) dt \right) = \lim_{\Delta t_k \rightarrow 0} \overleftarrow{\prod}_k e^{-i\mathcal{L}(t_k)\Delta t_k} \quad (2)$$

where $\mathbf{p}(t)$ is the density matrix, $\mathcal{L}(t)$ is the Liouvillian, $\mathcal{H}(t)$ is the Hamiltonian commutation superoperator, \mathcal{R} is the relaxation superoperator (not usually time-dependent), arrow over the exponential indicates Dyson time order [14], slices of duration Δt_k are centred around t_k , and the product is ordered from right to left in time.

2.1 Lie group methods

Computationally efficient extensions of this scheme to higher accuracy orders with respect to Δt_k are recent [15-17]. They go under the general name of Lie group methods [16]; their key feature is that the approximation is made at the level of the generator of the exponential action. Consider the general algebraic form of the Lie equation in the magnetic resonance notation:

$$\frac{d}{dt} \mathbf{p}(t) = -i\mathcal{L}(t, \mathbf{p})\mathbf{p}(t) \quad (3)$$

where \mathbf{p} is the state vector evolving under the (possibly dissipative, as well as time- and state-dependent) generator \mathcal{L} . Popular numerical methods for solving this equation (for example, Runge-Kutta [18,19]) do not observe essential conservation laws; they also fail on critical accuracy requirements (for example, trajectory endpoint phase) of quantum dynamics simulations.

It has been recognised for some time [15-17] that one class of numerical methods that does deliver on those requirements is based on the following reformulation of the time evolution problem:

$$\begin{aligned}\mathbf{p}(t) &= \exp\{\mathbf{\Omega}(t)\} \mathbf{p}(0) \\ \frac{d\mathbf{\Omega}}{dt} &= -i \sum_{m=0}^{\infty} \frac{B_m}{m!} \underbrace{[\mathbf{\Omega}, [\mathbf{\Omega}, \dots [\mathbf{\Omega}, \mathcal{L}]]]}_m, \quad \mathbf{\Omega}(0) = \mathbf{0}\end{aligned}\tag{4}$$

where B_k are Bernoulli numbers [20]. The series in the differential equation for $\mathbf{\Omega}(t)$ may be truncated and the equation then solved using standard numerical ODE methods [15-17]. The exponential action ensures that group-theoretical conservation laws are followed.

Using Magnus expansions [17,21] yields the following one-point, two-point (recently explored in the optimal control context by Dalgaard and Motzoi [22]), and three-point propagation rules in the case when the evolution generator \mathcal{L} is not state-dependent:

$$\begin{aligned}\mathbf{p} &\leftarrow \exp\{-i\mathcal{L}_M \Delta t\} \mathbf{p} \\ \mathbf{p} &\leftarrow \exp\left\{-i\left(\frac{\mathcal{L}_L + \mathcal{L}_R}{2} + \frac{i\sqrt{3}}{12} [\mathcal{L}_L, \mathcal{L}_R] \Delta t\right) \Delta t\right\} \mathbf{p} \\ \mathbf{p} &\leftarrow \exp\left\{-i\left(\frac{\mathcal{L}_L + 4\mathcal{L}_M + \mathcal{L}_R}{6} + \frac{i[\mathcal{L}_L, \mathcal{L}_R] \Delta t}{12}\right) \Delta t\right\} \mathbf{p}\end{aligned}\tag{5}$$

where L, R, and M subscripts indicate the left edge, the right edge, and the midpoint of the Δt interval; the one-point rule is identical to the established practice in Eqs (1) and (2). These rules are also applicable to isospectral flow problems (colloquially called “Hilbert space evolution” in magnetic resonance [23]) where the propagation step involves two-sided multiplication of the density matrix [17].

In situations when the evolution generator does depend on the state (radiation damping [24], relaxation theories at low temperature [25], non-linear chemical kinetics [26], *etc.*), the simplest (of many possibilities [15-17]) second order Lie group method estimates the generator at the midpoint, and uses the estimate to propagate:

$$\begin{aligned}\mathcal{L}_L &\leftarrow \mathcal{L}(t_L, \mathbf{p}_L) \\ \mathbf{p}_M &\leftarrow \exp\left(-\frac{i}{2}(t_R - t_L)\mathcal{L}_L\right) \mathbf{p}_L \\ \mathcal{L}_M &\leftarrow \mathcal{L}(t_M, \mathbf{p}_M) \\ \mathbf{p}_R &\leftarrow \exp\left(-i(t_R - t_L)\mathcal{L}_M\right) \mathbf{p}_L\end{aligned}\tag{6}$$

The simplest fourth order method proceeds to estimate the generator at the right edge and adds the following two stages to Eq (6):

$$\begin{aligned}\mathcal{L}_R &\leftarrow \mathcal{L}(t_R, \mathbf{p}_R) \\ \mathbf{p}_R &\leftarrow \exp\left\{-i\left(\frac{\mathcal{L}_L + 4\mathcal{L}_M + \mathcal{L}_R}{6} + \frac{i[\mathcal{L}_L, \mathcal{L}_R] \Delta t}{12}\right) \Delta t\right\} \mathbf{p}_L\end{aligned}\tag{7}$$

Other methods in this class differ in the details of the approximations used to solve Eq (4) for $\mathbf{\Omega}(t)$; a review was recently published by Iserles, Munthe-Kaas, Nørsett, and Zanna [16].

2.2 Numerically efficient implementations

When a propagator is computed explicitly, the additional cost of using two-and three-point rules in Eq (5) – two matrix multiplications – is negligible relative to the cost of the subsequent calculation of the matrix exponential. However, computing the exponential explicitly (cubic complexity with matrix dimension and much increased memory utilisation relative to storing only the generator) is rarely efficient, particularly in situations when the generator is defined implicitly, for example as a polyadic object with un-opened Kronecker products [27] or a DMRG-type tensor structure [28]. In those cases, only the product of \mathcal{L} with a user-specified vector is available, and Krylov type propagation algorithms [29] must be used – those are free of matrix-matrix multiplications. A simple illustration is the Taylor expansion of the action by the exponential of a matrix \mathbf{A} on a vector \mathbf{v} :

$$\exp(\mathbf{A})\mathbf{v} = \left[\sum_{k=0}^{\infty} \mathbf{A}^k / k! \right] \mathbf{v} = \sum_{k=0}^{\infty} \frac{1}{k!} \mathbf{A}(\mathbf{A} \cdots (\mathbf{A}\mathbf{v})) \quad (8)$$

where the right hand side is reordered to have only matrix-vector products. Those are cheaper (quadratic complexity with dimension) than matrix-matrix products involved in the Taylor series for the exponential of \mathbf{A} . This simple trick is in practice equivalent to Krylov methods, where the problem is projected into the Krylov subspace of \mathbf{A} and \mathbf{v} spanned by the set of products $\{\mathbf{v}, \mathbf{Av}, \mathbf{A}^2\mathbf{v}, \dots\}$, the product $\exp(\mathbf{A})\mathbf{v}$ is computed inside the Krylov subspace, and then projected back [29]. Eq (8) is a shortcut because the expansion coefficients of $\exp(\mathbf{A})\mathbf{v}$ in $\{\mathbf{v}, \mathbf{Av}, \mathbf{A}^2\mathbf{v}, \dots\}$ are already known.

Technical details are given in Chapter 4 of IK's book on the subject [30]. The simplicity of adapting this process for the two- and three-point rules in Eq (5) is illustrated by *Matlab* code of the inner loop in the summation of Eq (8). The midpoint code, where k is the summation variable, $t/nsteps$ is the subdivided time step, L is the Liouvillian, and `next_term` refers to the terms of the summation, is:

```
% Centre point propagator
next_term=-(1i/k)*(t/nsteps)*(L*next_term);
```

The two-point propagator adaptation of this code pre-computes $\mathcal{L}_L\mathbf{p}$ and $\mathcal{L}_R\mathbf{p}$, and re-uses them within the commutator; the overall complexity ends up being four matrix-vector multiplications per term of the Taylor series for the middle row of Eq (5):

```
% Re-usable intermediates
rho_a=L{1}*next_term; rho_b=L{2}*next_term;

% Left edge + right edge two-point propagator
next_term=-(1i/2)*(1/k)*(t/nsteps)*(rho_a+rho_b)+...
           (sqrt(3)/12)*(1/k)*(t^2/nsteps)*(L{1}*rho_b-L{2}*rho_a);
```

The three-point propagator in the bottom row of Eq (5), when similarly implemented, requires five matrix-vector multiplications per summation term. When the time step is appropriately scaled [30], the series converges quickly and monotonically in the norm. The implementation for the state-dependent generator case in Eqs (6) and (7) is similar, open-source code is available in *Spinach* [10].

2.3 Practical accuracy benchmarks

Even before their benefits in the context of optimal control theory are evaluated, the improvement in the accuracy (relative to the currently dominant piecewise-constant implementations) is so significant (Figure 2) that we recommend adopting these methods in all magnetic resonance simulation packages. Although Dalgaard and Motzoi are pessimistic in their conclusions section [22] about the logistical overhead of high-rank geometric integrators, a simple three-point integrator (last row of Eq (5) and yellow curve in Figure 2) does actually exist. We do share the pessimism for higher orders though. For a popular Veshtort-Griffin band-selective shaped pulse [31] in NMR spectroscopy, the accuracy of the three-point integrator at 50 time slices exceeds the piecewise-constant approximation at 1000 slices. This 20-fold saving factor pertains directly to Hilbert space evolution; for Liouville space Krylov propagation, it is reduced to 4-fold on the wall clock when we take into account the greater numerical cost of the three-point propagation step, but that is still a major efficiency improvement.

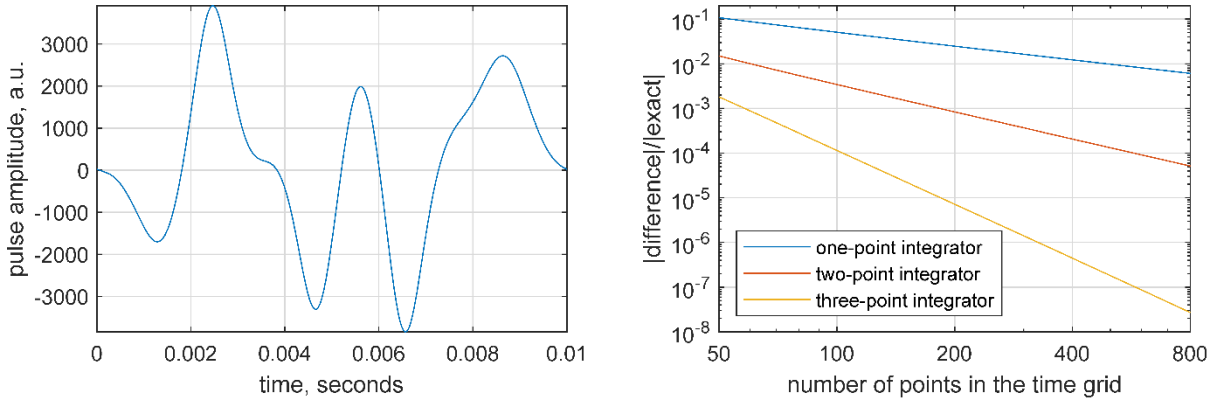


Figure 2. (Left) Veshtort-Griffin E1000B band-selective radiofrequency pulse used in NMR spectroscopy to achieve selective magnetisation excitation [31]. **(Right)** Final state accuracy as a function of discretisation point count using: (blue line) piecewise-constant approximation; (red line) two-point second-order Lie integrator in Eq (5); (yellow line) three-point fourth-order Lie integrator in Eq (5). Reproduced from the example set of Spinach library [10].

The same efficiency is seen in simulations involving state-dependent generators; a common example in magnetic resonance is radiation damping, for which the modified Bloch equations are [24]:

$$\frac{\partial}{\partial t} \begin{pmatrix} \mu_x \\ \mu_y \\ \mu_z \end{pmatrix} = \begin{pmatrix} -r_2 & -\omega & 0 \\ \omega & -r_2 & 0 \\ 0 & 0 & -r_1 \end{pmatrix} \begin{pmatrix} \mu_x \\ \mu_y \\ \mu_z - \mu_{eq} \end{pmatrix} - k_{rd} \begin{pmatrix} \mu_x \mu_z \\ \mu_y \mu_z \\ \mu_x^2 + \mu_y^2 \end{pmatrix} \quad (9)$$

where μ_{XYZ} are cartesian components of the magnetisation vector, ω is the Larmor frequency, $r_{1,2}$ are longitudinal and transverse relaxation rates, and k_{rd} is the radiation damping rate constant. Rewriting this equation in pseudolinear form exposes the state-dependent generator:

$$\frac{\partial}{\partial t} \begin{pmatrix} \mu_x \\ \mu_y \\ \mu_z \end{pmatrix} = - \begin{pmatrix} r_2 + k_{rd} \mu_z & \omega & 0 \\ -\omega & r_2 + k_{rd} \mu_z & 0 \\ k_{rd} \mu_x & k_{rd} \mu_y & r_1 \end{pmatrix} \begin{pmatrix} \mu_x \\ \mu_y \\ \mu_z \end{pmatrix} \quad (10)$$

which goes into Eqs (6) and (7). The accuracy profile is shown in Figure 3 – the scaling of the residual error is the same as it was for the state-independent generator in the right panel of Figure 2.

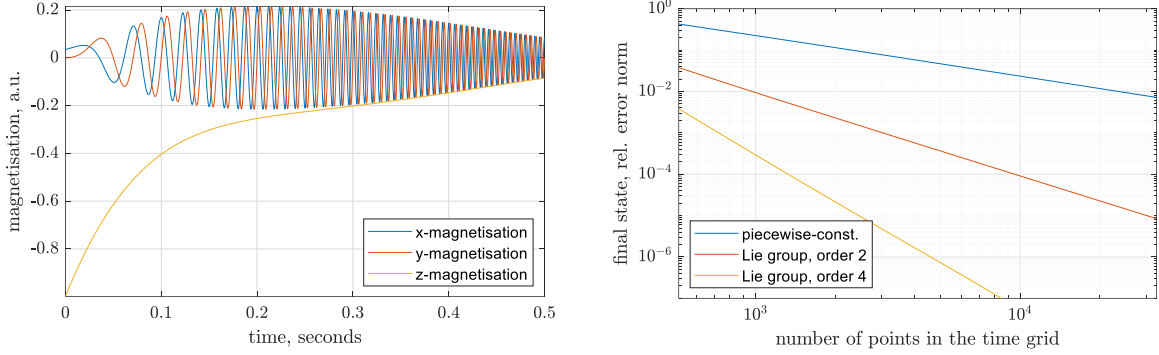


Figure 3. (Left) Rotating frame precession of an ensemble of magnetic dipoles in the presence of a linearly swept magnetic field (Zeeman frequency ramp from 0 to 200 Hz in 0.5 seconds), decoherence ($T_1 = T_2 = 0.1$ seconds), and radiation damping with $k_{rd} = 40$ Hz in Eq (9). The initial condition is off by 2 degrees from the negative direction of the Z axis. **(Right)** Relative error in the final state after propagation to $t = 0.5$ seconds using the indicated integrators. Reproduced from the example set of Spinach library [10].

3. Lie group extension of the GRAPE algorithm

Gradient ascent pulse engineering [1-3] is an open-loop quantum control framework that seeks to maximise measures of experiment fidelity with respect to instrumentally constrained control parameters. For common dissipative ensemble control problems, the equation of motion is:

$$\frac{d}{dt} \mathbf{p}(t) = -i\mathcal{L}(t)\mathbf{p}(t), \quad \mathcal{L}(t) = \mathcal{K}(t) + i\mathcal{R} \quad (11)$$

where \mathbf{p} is the ensemble state vector (typically a vectorised density matrix [23]), $\mathcal{K}(t)$ is the unitary evolution generator (typically the Hamiltonian commutation superoperator), and \mathcal{R} is the dissipative evolution generator. The Liouvillian $\mathcal{L}(t)$ may be split into the uncontrollable “drift” part $\mathcal{D}(t)$ and a linear combination of the operators \mathcal{C}_k whose coefficients $c^{(k)}(t)$ the instrument can vary:

$$\mathcal{L}(t) = \mathcal{D}(t) + \sum_k c^{(k)}(t) \mathcal{C}_k \quad (12)$$

For an experiment of duration T with initial condition \mathbf{p}_0 and the desired destination state $\mathbf{\delta}$, a popular measures of fidelity are functions of the overlap between $\mathbf{\delta}$ and $\mathbf{p}(T)$:

$$f = \langle \mathbf{\delta} | \mathbf{p}(T) \rangle = \langle \mathbf{\delta} | \overleftarrow{\exp} \left[-i \int_0^T \mathcal{L}(t) dt \right] | \mathbf{p}_0 \rangle \quad (13)$$

where the arrow indicates Dyson’s time-ordered exponential [14]. When this quantity and its variational derivatives with respect to the control sequences $c^{(k)}(t)$ are available from a simulation, the fidelity may be optimised. GRAPE [1] does this by discretising time and assuming both the drift and the control sequences to be piecewise-constant (Figure 4, left panel):

$$c^{(k)}(t) = c_n^{(k)}, \quad \mathcal{D}(t) = \mathcal{D}_n \quad (14)$$

$$t_{n-1} < t < t_n$$

This yields a remarkably efficient gradient evaluation algorithm reminiscent of backpropagation [32] in machine learning, wherein the gradient of the fidelity

$$\begin{aligned}
f &= \langle \delta | \mathcal{P}_N \cdots \mathcal{P}_{n+1} \mathcal{P}_n \mathcal{P}_{n-1} \cdots \mathcal{P}_1 | \mathbf{p}_0 \rangle \\
\frac{\partial f}{\partial c_n^{(k)}} &= \langle \delta | \mathcal{P}_N \cdots \mathcal{P}_{n+1} \frac{\partial \mathcal{P}_n}{\partial c_n^{(k)}} \mathcal{P}_{n-1} \cdots \mathcal{P}_1 | \mathbf{p}_0 \rangle \\
\mathcal{P}_n &= \exp \left[-i \left(\mathcal{D}_n + \sum_k c_n^{(k)} \mathcal{C}_k \right) \Delta t_n \right]
\end{aligned} \tag{15}$$

is calculated by one forward trajectory calculation from \mathbf{p}_0 , one backward trajectory calculation with Hermitian conjugate generators from δ , and a number of inner products with propagator derivatives in the middle [5]. The efficiency extends to arbitrary waveform basis sets. Consider a real orthonormal basis set of waveforms $\{\mathbf{w}_1, \dots, \mathbf{w}_M\}$:

$$\mathbf{W} = \begin{bmatrix} | & \cdots & | \\ \mathbf{w}_1 & \cdots & \mathbf{w}_M \\ | & \cdots & | \end{bmatrix}, \quad \mathbf{W}^T \mathbf{W} = \mathbf{1} \tag{16}$$

such that the control sequence $\mathbf{c}^{(k)}$ at k -th channel has an expansion

$$\mathbf{c}^{(k)} = \sum_m \alpha_m^{(k)} \mathbf{w}_m = \mathbf{W} \mathbf{a}^{(k)} \quad \Leftrightarrow \quad c_n^{(k)} = \sum_m w_{nm} \alpha_m^{(k)} \tag{17}$$

Then derivatives of any function f of $\mathbf{c}^{(k)}$ vector are translated as follows into the corresponding derivatives with respect to the waveform basis expansion coefficient vector $\mathbf{a}^{(k)}$:

$$\begin{aligned}
\frac{\partial f}{\partial \alpha_m^{(k)}} &= \sum_n \frac{\partial f}{\partial c_n^{(k)}} \frac{\partial c_n^{(k)}}{\partial \alpha_m^{(k)}} = \sum_n \frac{\partial f}{\partial c_n^{(k)}} w_{nm} \quad \Leftrightarrow \quad \nabla_{\mathbf{a}} f = \mathbf{W}^T [\nabla_{\mathbf{c}} f] \\
\frac{\partial^2 f}{\partial \alpha_m^{(k)} \partial \alpha_{m'}^{(k')}} &= \sum_{n,n'} \frac{\partial f}{\partial c_n^{(k)} \partial c_{n'}^{(k')}} w_{nm} w_{n'm'}
\end{aligned} \tag{18}$$

where m enumerates basis waveforms, n enumerates time points and k enumerates control channels. These are special cases of matrix calculus chain rules; these relations connect the methods that use waveform basis sets to GRAPE algorithms [1,2].

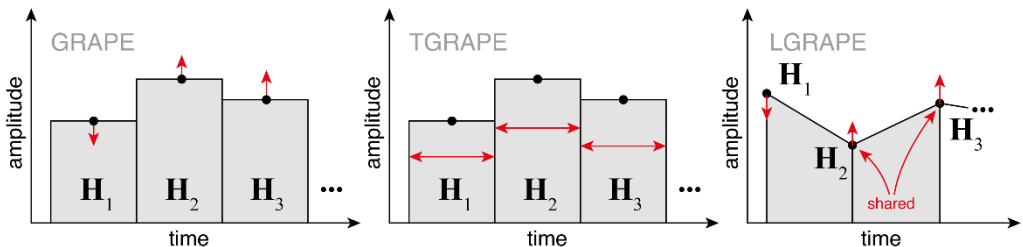


Figure 4. Schematic illustrations of the control sequence parameter update stage in GRAPE [1] (variation of piecewise-constant control coefficients, **left**), TGRAPE (Section 3.2, variation of slice durations with piecewise-constant control coefficients, **middle**), and of the extension of the same principle to continuous control sequences (Sections 2.1 and 3.1, piecewise-linear version shown, abbreviated LGRAPE, **right**).

Eq (15) critically relies on the piecewise-constant approximation; its shortcomings are described in the Introduction. An adaptation of the GRAPE framework to Lie group methods could alleviate the instrument response problem – the control sequence would no longer be piecewise-constant – but it would

also require the corresponding update to the mathematics and the logistics of Eq (15) because adjacent Hamiltonians would affect the evolution in more than one slice (Figure 4, right panel).

3.1 Control sequence derivatives

Under the two-point Lie group propagators in Eq (5), the expression for the fidelity is modified because each propagator now depends on two adjacent points of the discretised control sequence:

$$f = \langle \delta | \mathcal{P}_{N,N-1} \mathcal{P}_{N-1,N-2} \cdots \mathcal{P}_{2,1} \mathcal{P}_{1,0} | \mathbf{p}_0 \rangle, \quad \mathcal{L}_n = \mathcal{D}_n + \sum_k c_n^{(k)} \mathcal{C}_k$$

$$\mathcal{P}_{n+1,n} = \exp \left\{ -i \left(\frac{\mathcal{L}_n + \mathcal{L}_{n+1}}{2} + \frac{i\sqrt{3}}{12} [\mathcal{L}_n, \mathcal{L}_{n+1}] \Delta t \right) \Delta t \right\} \quad (19)$$

and adjacent propagators share a point. There are three types of derivatives in this setting – the first-point (one propagator), the last point (one propagator), and midpoint (two adjacent propagators):

$$\frac{\partial f}{\partial c_0^{(k)}} = \langle \delta | \mathcal{P}_{N,N-1} \mathcal{P}_{N-1,N-2} \cdots \mathcal{P}_{2,1} \left(\frac{\partial}{\partial c_0^{(k)}} \mathcal{P}_{1,0} \right) | \mathbf{p}_0 \rangle$$

$$\frac{\partial f}{\partial c_N^{(k)}} = \langle \delta | \left(\frac{\partial}{\partial c_1^{(k)}} \mathcal{P}_{N,N-1} \right) \mathcal{P}_{N-1,N-2} \cdots \mathcal{P}_{3,2} \mathcal{P}_{1,0} | \mathbf{p}_0 \rangle \quad (20)$$

$$\frac{\partial f}{\partial c_n^{(k)}} = \langle \delta | \mathcal{P}_{N,N-1} \mathcal{P}_{N-1,N-2} \cdots \left(\frac{\partial}{\partial c_n^{(k)}} (\mathcal{P}_{n+1,n} \mathcal{P}_{n,n-1}) \right) \cdots \mathcal{P}_{3,2} \mathcal{P}_{1,0} | \mathbf{p}_0 \rangle$$

For the first-point and the last-point propagators, the directional derivative problem is already solved [2,33]; numerical implementations are available in *Spinach* [10]. The midpoint propagator is reduced to the solved case by the application of matrix product rule:

$$\frac{\partial}{\partial c_n^{(k)}} (\mathcal{P}_{n+1,n} \mathcal{P}_{n,n-1}) = \left(\frac{\partial}{\partial c_n^{(k)}} \mathcal{P}_{n+1,n} \right) \mathcal{P}_{n,n-1} + \mathcal{P}_{n+1,n} \left(\frac{\partial}{\partial c_n^{(k)}} \mathcal{P}_{n,n-1} \right) \quad (21)$$

The problem is therefore reduced to calculating the derivatives of the propagator in Eq (19) with respect to the control coefficients. Consider a particular time interval with a left (L) and a right (R) time point. The Liouvillians and the two-point step generator are:

$$\mathcal{L} = \frac{\mathcal{L}_L + \mathcal{L}_R}{2} + \frac{i\sqrt{3}}{12} [\mathcal{L}_L, \mathcal{L}_R] \Delta t$$

$$\mathcal{L}_L = \mathcal{D}_L + \sum_k c_L^{(k)} \mathcal{C}_k, \quad \mathcal{L}_R = \mathcal{D}_R + \sum_k c_R^{(k)} \mathcal{C}_k \quad (22)$$

where $\mathcal{D}_{L,R}$ are drift generators, \mathcal{C}_k are control operators, $c_{L,R}^{(k)}$ are control coefficients, and the sum runs over control channels. After straightforward rearrangements and differentiation, we arrive at the following expressions for the derivatives of the Liouvillian with respect to the control coefficients:

$$\frac{\partial \mathcal{L}}{\partial c_R^{(k)}} = \left(\frac{\mathcal{C}_k}{2} + \frac{i\sqrt{3}\Delta t}{12} [\mathcal{D}_L, \mathcal{C}_k] \right) + \frac{i\sqrt{3}\Delta t}{12} \sum_n c_L^{(n)} [\mathcal{C}_n, \mathcal{C}_k]$$

$$\frac{\partial \mathcal{L}}{\partial c_L^{(k)}} = \left(\frac{\mathcal{C}_k}{2} + \frac{i\sqrt{3}\Delta t}{12} [\mathcal{C}_k, \mathcal{D}_R] \right) + \frac{i\sqrt{3}\Delta t}{12} \sum_n c_R^{(n)} [\mathcal{C}_k, \mathcal{C}_n] \quad (23)$$

These expressions are compatible with the cases where propagators and their partial derivatives are calculated explicitly using auxiliary matrices [33]:

$$\exp \left[\begin{pmatrix} \mathbf{A} & \partial \mathbf{A} / \partial \alpha \\ \mathbf{0} & \mathbf{A} \end{pmatrix} \right] = \begin{pmatrix} e^{\mathbf{A}} & \partial e^{\mathbf{A}} / \partial \alpha \\ \mathbf{0} & e^{\mathbf{A}} \end{pmatrix} \quad (24)$$

as well as with the cases where only their action on a vector is needed [3,33]. It bears notice (proof by induction for matrix powers, followed by Taylor series) that also:

$$f \left[\begin{pmatrix} \mathbf{A} & \partial \mathbf{A} / \partial \alpha \\ \mathbf{0} & \mathbf{A} \end{pmatrix} \right] = \begin{pmatrix} f(\mathbf{A}) & \partial f(\mathbf{A}) / \partial \alpha \\ \mathbf{0} & f(\mathbf{A}) \end{pmatrix} \quad (25)$$

for any single-valued scalar function $f(x)$ that can be extended to a matrix function using Taylor series. The bulkier case of the three-point propagation rule in Eq (5) is handled in the same way.

3.2 Time slice duration derivatives

An under-appreciated optimisation strategy within GRAPE framework is through variation of time slice durations (Figure 4, middle panel). Its practical value comes from dismal instrumental realities: once a particular experiment is running, adjusting time slices is typically the easiest thing to do because hardware non-linearities and calibration problems are absent.

Within the piecewise-constant original formulation of GRAPE [1], obtaining the gradient of the fidelity with respect to the slice duration vector τ is straightforward:

$$\begin{aligned} \frac{\partial f}{\partial \tau_n} &= \langle \mathbf{\delta} | \mathcal{P}_N \cdots \mathcal{P}_{n+1} \frac{\partial \mathcal{P}_n}{\partial \tau_k} \mathcal{P}_{n-1} \cdots \mathcal{P}_1 | \mathbf{p}_0 \rangle \\ \frac{\partial \mathcal{P}_n}{\partial \tau_k} &= \frac{\partial}{\partial \tau_k} \exp[-i\mathcal{L}_n \tau_n] = -i\mathcal{L}_n \exp[-i\mathcal{L}_n \tau_n] \end{aligned} \quad (26)$$

which is again compatible with the efficient implementation logistics described above – the system is propagated forward from the initial condition, backward from the destination state, and the matrix elements are calculated in a parallel loop:

$$\begin{aligned} \frac{\partial f}{\partial \tau_n} &= -i \langle \mathbf{\delta}_n | \mathcal{L}_n | \mathbf{p}_n \rangle, & \mathcal{P}_n &= \exp[-i\mathcal{L}_n \tau_n] \\ \langle \mathbf{\delta}_n | &= \langle \mathbf{\delta} | \mathcal{P}_N \cdots \mathcal{P}_{n-1}, & | \mathbf{p}_n \rangle &= \mathcal{P}_n \cdots \mathcal{P}_1 | \mathbf{p}_0 \rangle \end{aligned} \quad (27)$$

The extension to Lie propagators, in the case of the two-point rule in Eq (5), is:

$$\begin{aligned} \frac{\partial f}{\partial \tau_n} &= \langle \mathbf{\delta} | \mathcal{P}_{N,N-1} \mathcal{P}_{N-1,N-2} \cdots \frac{\partial \mathcal{P}_{n,n-1}}{\partial \tau_n} \cdots \mathcal{P}_{2,1} \mathcal{P}_{1,0} | \mathbf{p}_0 \rangle \\ \mathcal{P}_{n,n-1} &= \exp \left\{ -i \left(\frac{\mathcal{L}_{n-1} + \mathcal{L}_n}{2} + \frac{i\sqrt{3}}{12} [\mathcal{L}_{n-1}, \mathcal{L}_n] \tau_n \right) \tau_n \right\} \end{aligned} \quad (28)$$

The derivative of this propagator with respect to slice duration is straightforward. Consider an interval of duration τ with a left edge Liouvillian \mathcal{L}_L and a right edge Liouvillian \mathcal{L}_R . Eq (24) and its numerically efficient refinements [3,33] are directly applicable with:

$$\begin{aligned}
\mathbf{A} &= -i \left(\frac{\mathcal{L}_L + \mathcal{L}_R}{2} + \frac{i\sqrt{3}}{12} [\mathcal{L}_L, \mathcal{L}_R] \tau \right) \tau \\
\frac{\partial \mathbf{A}}{\partial \tau} &= -i \frac{\mathcal{L}_L + \mathcal{L}_R}{2} + \frac{\sqrt{3}}{6} [\mathcal{L}_L, \mathcal{L}_R] \tau
\end{aligned} \tag{29}$$

The three-point scheme in Eq (5) is handled in the same way. An open-source numerical implementation of slice-duration GRAPE is available in *Spinach* [10].

3.3 Practical benchmarks: broadband pulse

Consider a 90-degree universal rotation ^{13}C pulse in a modern 28.2 Tesla (1.2 GHz proton frequency) NMR magnet. The pulse must accomplish the following transformation of the basis operators:

$$\mathbf{S}_z \rightarrow \mathbf{S}_x, \quad \mathbf{S}_y \rightarrow \mathbf{S}_y, \quad \mathbf{S}_x \rightarrow -\mathbf{S}_z \tag{30}$$

uniformly within a bandwidth of around 200 ppm (≈ 60 kHz) and must be short enough for the worst-case ^{13}C - ^1H J -coupling (around 200 Hz) to have a negligible effect. The latter requirement caps the pulse duration at about $1/100J = 50 \mu\text{s}$. Maximum instrumentally achievable nutation frequency varies from 50 to 70 kHz across the radiofrequency coil of the NMR probe, and it is therefore clear that a hard ^{13}C pulse (*i.e.* the shortest pulse at the maximum available RF power, here about 4 μs) is not possible in a 1.2 GHz magnet due to significant phase errors across the spectral window (Figure 5, top panel). A key advantage of optimal control theory is the ability [5] to generate pulse waveforms that are: (a) free of such errors; (b) more resistant to resonance offset and power miscalibration than composite pulses; (c) able to accommodate secondary considerations, such as keyhole subspaces and dead times [30]. Optimal control pulses are longer than hard pulses, but they still fit comfortably into the timing window imposed by J -couplings; an example is shown in the bottom panel of Figure 5.

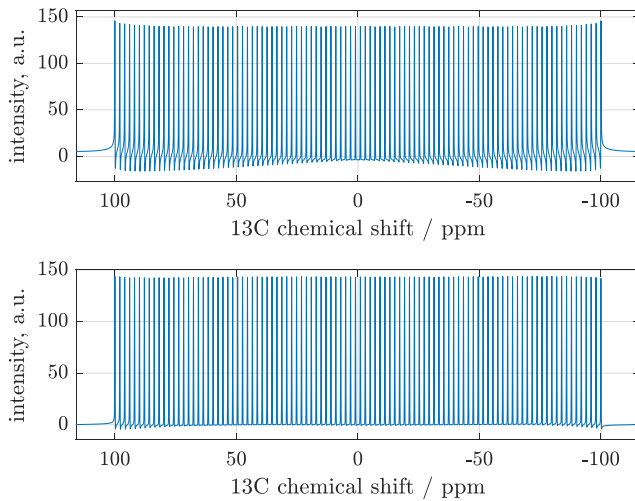


Figure 5. The effect of universal rotation pulses intended to accomplish the state space transformation in Eq (30) for an ensemble of 100 ^{13}C nuclei (spread uniformly over a ± 100 ppm interval) in a 28.2 Tesla (1.2 GHz proton frequency) NMR magnet. **Top panel:** ^{13}C NMR spectrum following a 4.2 μs hard pulse at 60 kHz nutation frequency, which is the limit of currently available hardware. **Bottom panel:** ^{13}C NMR spectrum following a 40 μs piecewise-constant optimal control pulse with 400 time slices, designed to maintain the same accuracy in the nutation frequency interval between 50 and 70 kHz. See [5] for further information on such pulses; the code generating this figure is available as a part of the example set of *Spinach* 2.8 and later.

In this section, we demonstrate that piecewise-linear versions of such pulses are never worse (in either convergence or performance), and in some circumstances are better than piecewise-constant versions; this is illustrated in Figure 6. The two panels on the left are “spaghetti plots”, giving the infidelity as a function of LBFGS-10 iteration count for the pulse described in the caption of Figure 5: it is clear that there is no significant difference in convergence behaviour between the standard piecewise-constant LBFGS-GRAPE [2] and its piecewise-linear extension; the same behaviour is observed for a few dozen other optimal control problems in the example set of *Spinach*. The panel on the right demonstrates that, for pulses with few time intervals, the piecewise-linear version of GRAPE outperforms the piecewise-constant one. For finely discretised pulses, the difference disappears because highly optimal and parameter distribution resilient universal rotation pulses tend to be smooth. Thus, the piecewise-linear version of GRAPE is advantageous in tightly timed experiments where the instrument only permits a small number of time slices.

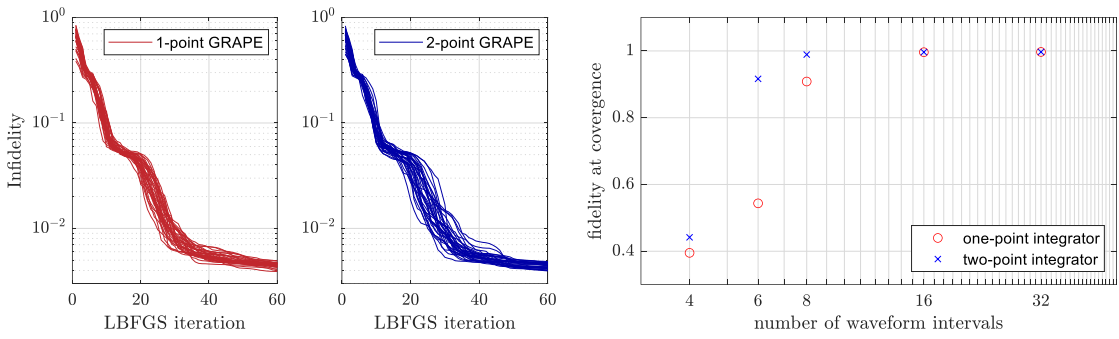


Figure 6. Relative performance illustrations for piecewise-constant (parameterised by one point per time interval) and piecewise-linear (parameterised by two points per time interval) GRAPE algorithms for the ^{13}C excitation pulse described in Section 3.3 of the main text. **Left and middle panel:** “spaghetti plots” illustrating LBFGS convergence behaviour of the two versions of GRAPE for a phase-modulated pulse with 60 time intervals, starting from a random initial guess. The convergence behaviour is essentially identical. **Right panel:** fidelity at convergence as a function of the number of intervals in the waveform for a phase-modulated pulse with the overall duration of 51.2 μs . The more flexible piecewise-linear version of GRAPE advocated in this paper shows better performance with fewer time discretisation intervals.

3.4 Practical benchmarks: prephasing pulse

An important use case for optimal control theory is dead time elimination: a control sequence may be designed to set the dynamics up for arriving at the desired destination *some time after* the controls are switched off. In magnetic resonance, this is beneficial for NMR of low- γ nuclei (because RLC circuit response effects are stronger at lower frequencies) and for quadrupolar NMR of solid powders (because of rapid ensemble dephasing by nuclear quadrupolar interaction). In both cases, the sweep width of the spectrum can be in the MHz, necessitating sub-microsecond time slices. Short time slices then render the pulses vulnerable to the distortions introduced by the RLC circuit of the probe.

Here we model the NMR probe, as a series RLC circuit; this is a rough approximation, but it is expected to capture the differences between piecewise-constant and piecewise-linear (in the rotating frame) pulse input. The transfer function is obtained from a combination of Kirchhoff’s first law [34], Ohm’s law [35], inductor equation, and capacitor equation [36]:

$$\begin{aligned} V_{\text{IN}}(t) &= V_{\text{R}}(t) + V_{\text{L}}(t) + V_{\text{C}}(t) \\ V_{\text{R}}(t) &= RI(t), \quad V_{\text{L}}(t) = LI'(t), \quad I(t) = CV_{\text{C}}'(t) \end{aligned} \quad (31)$$

where primes indicate time derivatives, V_{IN} is input voltage, R is the resistance of the resistor, C is the capacitance of the capacitor, L is the inductance of the inductor, I is current in the circuit, and $V_{\{R,L,C\}}$ are voltages across the resistor, inductor, and capacitor, respectively. For zero initial conditions in the Laplace domain, the corresponding equations are:

$$\begin{aligned} V_{\text{IN}}(s) &= V_R(s) + V_L(s) + V_C(s) \\ V_R(s) &= RI(s), \quad V_L(s) = sLI(s), \quad I(s) = sCV_C(s) \end{aligned} \quad (32)$$

The quantity seen by the spin system is the magnetic field generated within the inductor, that quantity is proportional to the current. Thus, the transfer function of interest is:

$$T(s) \propto I(s)/V_{\text{IN}}(s) \propto \frac{Q^{-1}\omega_0^{-1}}{\omega_0^{-2}s^2 + Q^{-1}\omega_0^{-1}s + 1} \quad (33)$$

where $\omega_0 = 1/\sqrt{LC}$ is the resonance frequency and $Q = \sqrt{L/C}/R$ is the quality factor. In practice, each pulse was transformed from the rotating frame into the laboratory frame by mixing it with the carrier frequency ω_0 , then supplied to Matlab Control System Toolbox alongside the transfer function in Eq (33), and the response then heterodyned numerically back into the rotating frame. Documented source code is available (retrans.m) as a part of *Spinach* library versions 2.8 and later.

The test case was a ^2H excitation pulse in a 14.1 T magnet, designed to set transverse deuterium magnetisation in $-\text{CD}_3$ alanine powder up for refocussing 100 μs after the end of the pulse. The quadrupole interaction tensor anisotropy (partially averaged by rapid methyl group rotation in the room temperature solid) is around 40 kHz [37]. A pulse with 24 equal time slices, overall duration of 156 μs and the maximum nutation frequency of 35 kHz per channel was optimised with the first two and the last two pulse discretisation points frozen at zero to comply with the response theory assumptions in Eqs (31)-(33). The optimisation was carried out simultaneously for 200 uniformly distributed orientations obtained from the REPULSION procedure [38] using its implementation in *Spinach* [10]. RLC distortions with $Q = 200$ and ω_0 set to deuterium Larmor frequency were then applied to both waveforms.

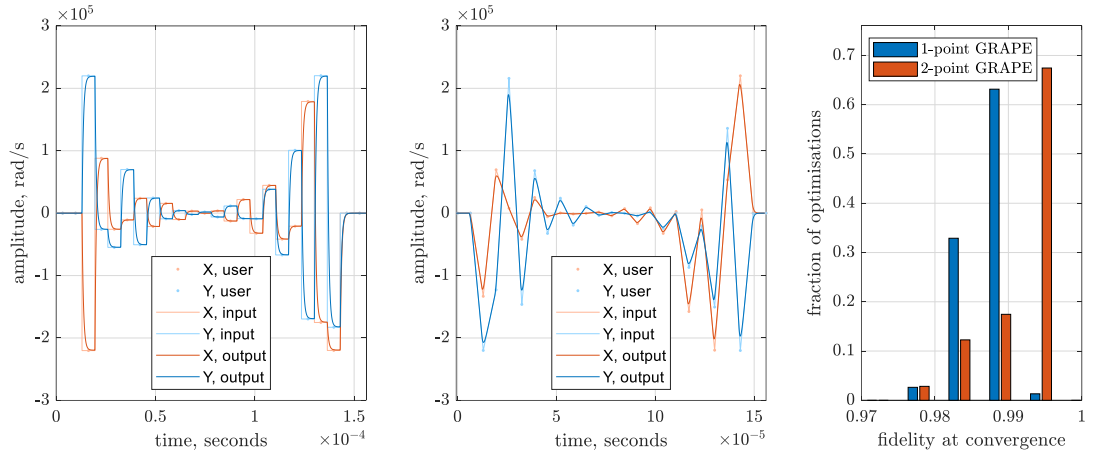


Figure 7. An illustration of the fact that piecewise-constant composite NMR pulses suffer greater RLC circuit distortions and yield smaller fidelities at convergence than piecewise-linear pulses. Faint orange and blue lines indicate RLC circuit inputs, strong lines indicate the outputs after the RLC distortion with $Q=200$ is applied. **Left panel:** a conventional piecewise-constant NMR pulse, designed using GRAPE [1] to start with longitudinal magnetisation and produce perfect refocussing of transverse ^2H magnetisation in $-\text{CD}_3$ alanine powder 100 μs after the end of the pulse. **Middle panel:** a piecewise-linear pulse, designed using the method proposed in this paper and plotted with RLC time

delay compensation, accomplishing the same objective. Right panel: fidelity-at-convergence histograms for 200 pulses optimised from random initial guesses using 1-point and 2-point versions of the GRAPE algorithm.

Several hundred piecewise-constant (Figure 7, left panel) and piecewise-linear (Figure 7, middle panel) pulses were obtained by starting the optimisation from different random initial guesses. It is clear from Figure 7 that piecewise-linear pulses suffer less from RLC circuit distortions and yield higher fidelities at convergence than piecewise-constant ones. In our hands (however, see also [22]), the difference in performance between the two types of pulses is not dramatic, and only manifests for tightly timed pulses accomplishing difficult objectives.

5. Conclusions

The historically dominant piecewise-constant approximation for shaped magnetic resonance pulses was in some ways the worst possible choice. From the mathematical point of view, it corresponds to the lowest accuracy Lie group integrator; from the engineering side, it creates the worst possible RLC response transients. It has been clear for some time [16,17,22,39] that two- and three-point Lie integrators provide dramatically greater accuracy with only a modest increase in logistical and computational costs; here we have added a number of practical efficiency improvements in the context of quantum optimal control and NMR spectroscopy, and reported an implementation in the open-source *Spinach* library [10] for spin dynamics simulations. The corresponding modifications to the GRAPE framework, including integration with LBFGS, ensemble control, and dissipative control problems, are available in versions 2.8 and later of that library.

Acknowledgements

This work was supported by EPSRC (EP/W020343/1) and MathWorks, and used NVIDIA Tesla A100 GPUs through NVIDIA Academic Grants Programme. We are grateful to Jos Martin, Raymond Norris, and Alison Eele for expert technical support with Parallel Matlab. The authors acknowledge the use of the IRIDIS High Performance Computing Facility, and associated support services at the University of Southampton, in the completion of this work.

References

- [1] N. Khaneja, T. Reiss, C. Kehlet, T. Schulte-Herbrüggen, S.J. Glaser, Optimal control of coupled spin dynamics: design of NMR pulse sequences by gradient ascent algorithms, *Journal of magnetic resonance*, 172 (2005) 296-305.
- [2] P. de Fouquieres, S.G. Schirmer, S.J. Glaser, I. Kuprov, Second order gradient ascent pulse engineering, *Journal of Magnetic Resonance*, 212 (2011) 412-417.
- [3] D.L. Goodwin, I. Kuprov, Modified Newton-Raphson GRAPE methods for optimal control of spin systems, *The Journal of chemical physics*, 144 (2016) 204107.
- [4] M.S. Vinding, D.L. Goodwin, I. Kuprov, T.E. Lund, Optimal control gradient precision trade-offs: Application to fast generation of DeepControl libraries for MRI, *Journal of Magnetic Resonance*, 333 (2021) 107094.
- [5] T.E. Skinner, T.O. Reiss, B. Luy, N. Khaneja, S.J. Glaser, Application of optimal control theory to the design of broadband excitation pulses for high-resolution NMR, *Journal of Magnetic Resonance*, 163 (2003) 8-15.
- [6] P. Coote, W. Bermel, H. Arthanari, Optimization of phase dispersion enables broadband excitation without homonuclear coupling artifacts, *Journal of Magnetic Resonance*, 325 (2021) 106928.

- [7] J. Saywell, M. Carey, M. Belal, I. Kuprov, T. Freegarde, Optimal control of Raman pulse sequences for atom interferometry, *Journal of Physics B: Atomic, Molecular and Optical Physics*, 53 (2020) 085006.
- [8] J. Saywell, M. Carey, I. Kuprov, T. Freegarde, Biselective pulses for large-area atom interferometry, *Physical Review A*, 101 (2020) 063625.
- [9] Z. Tošner, M.J. Brandl, J. Blahut, S.J. Glaser, B. Reif, Maximizing efficiency of dipolar recoupling in solid-state NMR using optimal control sequences, *Science advances*, 7 (2021) eabj5913.
- [10] H.J. Hogben, M. Krzstyniak, G.T. Charnock, P.J. Hore, I. Kuprov, Spinach – a software library for simulation of spin dynamics in large spin systems, *Journal of Magnetic Resonance*, 208 (2011) 179-194.
- [11] R.R. Ernst, G. Bodenhausen, A. Wokaun, *Principles of nuclear magnetic resonance in one and two dimensions*, 1987.
- [12] M. Mehring, V.A. Weberruss, *Object-oriented magnetic resonance: classes and objects, calculations and computations*, Elsevier, 2012.
- [13] Z. Tošner, T. Vosegaard, C. Kehlet, N. Khaneja, S.J. Glaser, N.C. Nielsen, Optimal control in NMR spectroscopy: numerical implementation in SIMPSON, *Journal of Magnetic Resonance*, 197 (2009) 120-134.
- [14] F.J. Dyson, The radiation theories of Tomonaga, Schwinger, and Feynman, *Physical Review*, 75 (1949) 486-502.
- [15] H. Munthe-Kaas, Runge-Kutta methods on Lie groups, *BIT Numerical Mathematics*, 38 (1998) 92-111.
- [16] A. Iserles, H.Z. Munthe-Kaas, S.P. Nørsett, A. Zanna, Lie-group methods, *Acta numerica*, 9 (2000) 215-365.
- [17] F. Casas, A. Iserles, Explicit Magnus expansions for nonlinear equations, *Journal of Physics A: Mathematical and General*, 39 (2006) 5445.
- [18] C. Runge, Über die numerische Auflösung von Differentialgleichungen, *Mathematische Annalen*, 46 (1895) 167-178.
- [19] W. Kutta, Beitrag zur naherungsweisen Integration totaler Differentialgleichungen, *Zeitschrift für Mathematik und Physik*, 46 (1901) 435-453.
- [20] J. Bernoulli, Ars conjectandi, *Impensis Fratrum Thurnisiorum*, 1713.
- [21] W. Magnus, On the exponential solution of differential equations for a linear operator, *Communications on pure and applied mathematics*, 7 (1954) 649-673.
- [22] M. Dalgaard, F. Motzoi, Fast, high precision dynamics in quantum optimal control theory, *Journal of Physics B: Atomic, Molecular and Optical Physics*, 55 (2022) 085501.
- [23] A.D. Bain, J.S. Martin, FT NMR of nonequilibrium states of complex spin systems, Part I: a Liouville space description, *Journal of Magnetic Resonance*, 29 (1978) 125-135.
- [24] A. Vlassenbroek, J. Jeener, P. Broekaert, Radiation damping in high resolution liquid NMR: a simulation study, *The Journal of chemical physics*, 103 (1995) 5886-5897.
- [25] A. Chessari, S.F. Cousin, S. Jannin, Q. Stern, The role of electron polarization on nuclear spin diffusion, *arXiv preprint arXiv:2206.14771*, (2022).
- [26] R.O. Kühne, T. Schaffhauser, A. Wokaun, R.R. Ernst, Study of transient chemical reactions by NMR: fast stopped-flow Fourier transform experiments, *Journal of Magnetic Resonance*, 35 (1979) 39-67.
- [27] A.J. Allami, P. Lally, I. Kuprov, Quantum mechanical MRI simulations: Solving the matrix dimension problem, *Science Advances*, 5 (2019) eaaw8962.
- [28] U. Schollwöck, The density-matrix renormalization group in the age of matrix product states, *Annals of physics*, 326 (2011) 96-192.

- [29] R.B. Sidje, *Expokit*: a software package for computing matrix exponentials, *ACM Transactions on Mathematical Software*, 24 (1998) 130-156.
- [30] I. Kuprov, *Spin*, Springer, 2023.
- [31] M. Veshtort, R.G. Griffin, High-performance selective excitation pulses for solid- and liquid-state NMR spectroscopy, *ChemPhysChem*, 5 (2004) 834-850.
- [32] D.E. Rumelhart, G.E. Hinton, R.J. Williams, Learning representations by back-propagating errors, *nature*, 323 (1986) 533-536.
- [33] D.L. Goodwin, I. Kuprov, Auxiliary matrix formalism for interaction representation transformations, optimal control, and spin relaxation theories, *The Journal of chemical physics*, 143 (2015) 084113.
- [34] G. Kirchhoff, Ueber die Auflösung der Gleichungen, auf welche man bei der Untersuchung der linearen Vertheilung galvanischer Ströme geführt wird, *Annalen der Physik*, 148 (1847) 497-508.
- [35] G.S. Ohm, *Die galvanische kette: mathematisch bearbeitet*, TH Riemann, 1827.
- [36] M. Faraday, Experimental researches in electricity: reprinted from the *Philosophical Transactions of 1831-1843*, 1846-1852, R&JE Taylor, 1839.
- [37] K. Beshah, E.T. Olejniczak, R.G. Griffin, Deuterium NMR study of methyl group dynamics in L-alanine, *The Journal of chemical physics*, 86 (1987) 4730-4736.
- [38] M. Bak, N.C. Nielsen, REPULSION, a novel approach to efficient powder averaging in solid-state NMR, *Journal of Magnetic Resonance*, 125 (1997) 132-139.
- [39] C.J. Budd, A. Iserles, Geometric integration: numerical solution of differential equations on manifolds, *Philosophical Transactions of the Royal Society of London. Series A: Mathematical, Physical and Engineering Sciences*, 357 (1999) 945-956.